# NUMERICAL INVESTIGATION OF SUBSONIC HYDROGEN JET RELEASE

**[1]Chernyavsky, B., [1]Benard P. , [2]Oshkai, P. and [2]Djilali, N.**

**[1]Institut de recherche sur l'hydrogène, Université du Québec à Trois-Rivières 3351, boulevard des Forges, C.P. 500 Trois-Rivières, Québec, Canada G9A 5H7, Boris.Chernyavsky@uqtr.ca**
**[2]Institute for Integrated Energy Systems, and Department of Mechanical Engineering, University of Victoria, Victoria, BC, V8W 3P6, Canada**

## ABSTRACT
A buoyant round vertical hydrogen jet has been investigated using Large Eddy Simulations at low Mach number. The influence of the transient concentration fields on the extent of the gas envelope with concentration within the flammability limits has been investigated, and their structure has been characterized. Investigation of the lower computational cost alternatives have been conducted.

## 1.0 INTRODUCTION
One of the significant hurdles in the way of large scale deployment of hydrogen powered road vehicles is the absence of well established guidelines covering the safety aspects of hydrogen storage, fueling and potential emergency scenarios. One of the important issues in formulating such guidelines is the understanding of an evolution of hydrogen concentration field, resulting from the controlled or uncontrolled release of hydrogen [1]. In order to guide the formulation of industrial codes and standards addressing hydrogen storage and transport, it is necessary to achieve better understanding of the physics associated with the development and behavior of the hydrogen jets.

The behavior of a round free jet had been a subject of a large number of both numerical and experimental studies ([2] – [5], among others), resulting in improved understanding of its development and characteristics. The remaining problems requiring further investigation include characterization and understanding of evolution of transient regimes over a wide range of both subsonic and supersonic initial release velocities; the effects of turbulence on the jet breakups, the effects of buoyancy, and the influence of adjacent solid surfaces. The inherent danger of hydrogen/air mixture in terms of flammability makes the experimental study of hydrogen release difficult and expensive. Thus, numerical simulations have become a tool of choice for the investigation of physical phenomena associated with such release. Large Eddy Simulation (LES) methodology had been previously successfully applied to the jet release problems in, among other, [6] and [7]. Present work utilizes LES approach coupled with the Smagorinsky subgrid scale (SGS) model, which has been previously successfully applied to a (non-buoyant) jet exhaust problem by [7] for a wide range of Reynolds numbers and exhaust velocities.

The present work is a continuation of the numerical and experimental study concentrating on investigation of the momentum dominated region of the moderately subsonic buoyant round jet. The primary objective is to use the high-fidelity numerical simulations and experiments in order to 1) improve the understanding of the interaction between turbulence, buoyancy, entrainment and nearby surface effects and the combined impact of these phenomena on jet spreading, mixing and therefore concentration fields, and 2) to determine what degree of simulation fidelity is necessary to obtain the data required for practical needs, with a particular view on safety applications. The research addressed moderately subsonic (M ~ 0.3) gas release, primarily within the momentum-dominated regime, which allowed to use high-fidelity simulations within a reasonable timeframe. It therefore occupied a less

explored area between a large body of works, concentrating on the supersonic regimes (cf. [6], [8] etc.), and investigations covering a very low speed releases, where the gas can be considered essentially incompressible, and the concentration field evolution is governed primarily by the mixing with small or non-existent momentum-dominated area ( cf. [3], [9]). While the emphasis on the high speed gas releases is justified since it has been shown [1], [7] that the supersonic regime would be dominant during most of the venting from the compressed vessels used in automotive applications, subsonic regime remains important for a number of problems, since it can significantly alter the concentration fields at the later stages of gas release and in the far field of the jet, e.g., through the increased importance of buoyancy relative to momentum effects. Subsonic cases are also important for consideration of the leak scenarios (when compressed vessel structural integrity is preserved), as well as for more violent releases from storage facilities, caused by the breach of thermal insulation and associated vaporization and subsequent escape of the stored hydrogen, with vaporization rates driving the exhaust conditions.

The present work builds on the results obtained during first part of the project [10], continued investigation of buoyant jet release through a round opening, corresponding to a case of a controlled release with fixed inflow boundary conditions. The focus of the preceding work was validation of numerical methods by comparison of data with in-house experimental results obtained using Particle Image Velocimetry (PIV) technique, and exploration of transient concentration fields (see, e.g., [11] and [12] for further discussion of transient fields), which are relatively poorly studied while presenting significant interest for safety applications. In order to perform comparison with the experiment, the earlier simulation [10] used helium jet in place of the hydrogen, with regions with gas within 4 - 75% designated as "flammable" conditions. The simulation used a popular Fluent numerical solver. The present work continues focusing on the investigation of the evolution of concentration field regions with gas concentration within flammability threshold, with a particular emphasis on the evolution of the transient concentration fields, while switching from helium (used previously to facilitate validation) to hydrogen, while simultaneously improving grid resolution in order to improve turbulence modeling. High computational cost, required for LES forced switch to alternative numerical solver, providing higher performance and allowing to use larger number of processors to further improve grid resolution while reducing calculation time. The high computational cost of LES also prompted an evaluation of alternative, simplified approaches, in a view of estimating their applicability for industry-level modeling. Regions with instantaneous gas concentration within the flammability limits had been monitored, and the structure and evolution of outlying transient gas pockets has been investigated along with the cumulative volume of such transient flammable regions.

## 2.0 GOVERNING EQUATIONS AND NUMERICAL SOLVER

Present simulations are performed using Structured PArallel Research Code (SPARC) originally developed in University of Karlsruhe [13]. This code had been extensively validated and demonstrated good agreement with experimental results for a wide variety of fluid dynamics problems. It provides high performance and good scalability, allowing parallelization through domain decomposition, necessary for high resolution LES within an acceptable time frame SPARC numerical solver numerically solves a system of mass, momentum and energy conservation equations (1-3) using the finite volume method:

$$\iiint_V \frac{\partial \rho}{\partial t} dV + \iint_S \rho \vec{v} \cdot \vec{n} dS = 0, \quad (1)$$

$$\iiint_V \frac{\partial (\rho \vec{v})}{\partial t} dV + \iint_S \rho \vec{v} (\vec{v} \cdot \vec{n}) dS + \iint_S p \vec{n} dS - \iint_S \vec{n} \cdot \bar{\bar{T}} dS = \iiint_V \rho \vec{g} dV, \quad (2)$$

$$\iiint_V \frac{\partial (\rho E)}{\partial t} dV + \iint_S \rho E (\vec{v} \cdot \vec{n}) dS + \iint_S p (\vec{v} \cdot \vec{n}) dS - \iint_S \vec{v} (\vec{n} \cdot \bar{\bar{T}}) dS + \iint_S \vec{n} \cdot \vec{q} dS = 0, \quad (3)$$

where $E$ is the total specific energy, $\vec{q}$ is the energy flux vector, and $\overline{T}$ is the viscous stress tensor. An explicit Runge-Kutta scheme is used for the time discretization. The Smagorinsky-Lilly SGS model is used for turbulence modeling, which gives the turbulent eddy viscosity as [14]:

$$\nu_t = (C_s\overline{\Delta})^2\sqrt{2\overline{S}_{ij}\overline{S}_{ij}} \quad (4)$$

where $\nu_t$ is the turbulent eddy viscosity, $C_s$ is the Smagorinsky constant, $\overline{\Delta}$ is the filter width and $S_{ij}$ is the strain rate tensor.

Numerical simulations have been performed for a vertical hydrogen jet with initial release velocity corresponding to M = 0.3. The computations were performed using a highly refined multiblock grid consisting of a cylinder representing an internal part of the injection nozzle and a frustum shaped external region. The cylinder simulates the outer portion of the nozzle and serves to generate a realistic flowfield at the nozzle exit. It has a diameter ($D$) of 5 mm and a similar length, with the pressure inlet boundary condition at the open exit and no slip boundaries on the walls. The inlet pressure and initial turbulence and velocity conditions are chosen to generate the realistic velocity and turbulence profiles at the nozzle exit (Fig. 1). The grid was significantly refined and improved from the original used in [10]. An updated grid contains approximately 3,000,000 cells, with the resolution in the mixing region near the exit from the nozzle chosen based on a local Kolmogorov scale. The grid geometry and expansion rate was chosen to follow expected evolution of the jet, based on the data reported in the literature and observed in previous numerical and experimental results [10].

The main computation domain consists of a frustum with a base diameter of 10 $D$, an outer diameter of 70 $D$, and a height of 38 $D$. The base of the frustum is set to a no-slip condition, while the sides are set to the pressure inlet condition to allow for entrainment. Outer boundary of the frustum is set to a pressure outlet condition. The cross section and general configuration of the grid are shown in Fig. 1. O-type grid is employed to avoid singularity at the jet axis, with transition between internal square and external radial grids well within inlet core. The flow was allowed to develop until it reached quasi-steady state, after which simulations were performed for four fluid particle flow-through times to obtain the turbulence statistics.

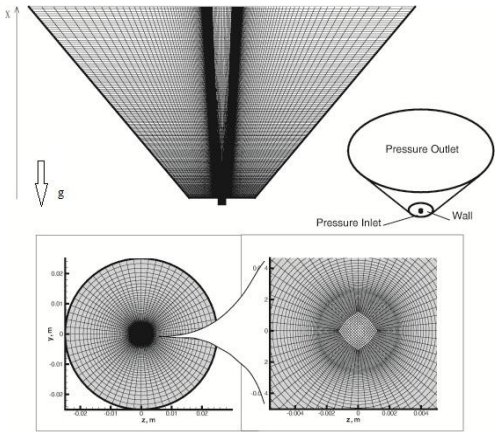


Figure 1. Schematic of the computational domain and grid cross section at $x$=0. Unshaded central area corresponds to the inflow boundary, shaded to the wall boundary condition

## 3.0 RESULTS AND DISCUSSION

### 3.1 Large Eddy Simulation of hydrogen jet: velocity and concentration fields

The first task of the present work was to extend the simulation performed in [10] to the hydrogen jet using improved grid. Figure 2a illustrates the inverse centerline velocity decay $u_j/u_c$, as a function of the downstream distance *x/D* for the hydrogen jet along with the numerical results for helium jet obtained using Fluent software [10] and its comparison with experimental results for air and helium jets obtained using Particle Image Velocimetry (PIV) method. Its shape suggests the presence of a short (~ 2 *x/D*) potential core followed by the transition to the self-similarity region. The variation of $u_c$ in the expansion region appears to be linear, conforming to $u_c^{-1} \sim x$ relationship, at $x/D > 3$ with different slopes for the different density jets. The transition occurs somewhat earlier than for helium, and particularly, air jets. The virtual origin for the numerical simulation $x_{vo}$ = -1.53 *x/D*. For comparison, the virtual origin of the helium jet was $x_{vo}$ = -0.3 *x/D* for LES simulation and approximately $x_{vo}$ = -0.2 *x/D* in the experiment. The coefficient $C_1$ from the relation $L_u/d=C_1(x-x_{v01})/d$ was calculated to be 0.18, compared to 0.11 observed for helium jet. The coefficient of the axial velocity decay *A* calculated from the expression $u_{jj}/u_c=2A((x-x_{vo})/D_{ef})$ was 0.098. These values are consistent with the jet spread rate calculated by the half-velocity width $L_u$ and velocity decay rate results obtained for helium and air jets.

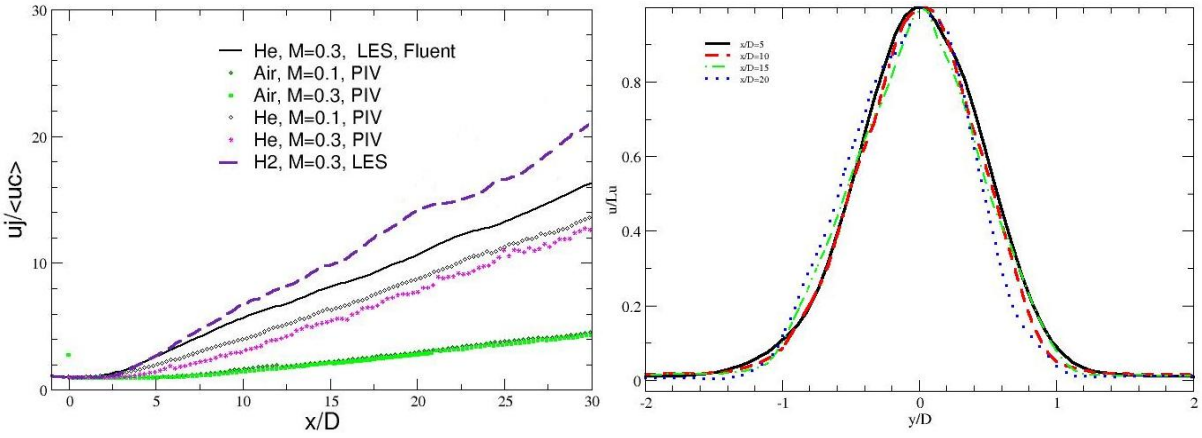


Figure 2. a) Jet spread rate $u_j/\langle u_c\rangle$ versus *x/D*, LES (SPARC and Fluent) and PIV; b) hydrogen normalized mean velocity profiles $\langle u\rangle/\langle u_c\rangle$ *versus* $y/L_u$ at various distances from the nozzle *x/D*.

An analysis of the radial mean longitudinal velocity profiles at various distances from the jet origin has been performed in order to confirm that the jet had reached fully developed stage and the statistic collection time was adequate. As can be seen in Fig. 2b, although it has been shown that an exact self-similarity cannot be achieved in buoyant flows [15], the radial profiles of the mean velocity normalized by the centerline mean velocity at *x/D* = 5, 10, 15 and 20 collapse well and can be reasonably approximated by Gaussian distribution $\langle u\rangle/\langle u_c\rangle = e^{-(r/Lu)^{\wedge}2\ln 2}$. The axial evolution of the rms ($u'=\langle u^2\rangle^{1/2}$ and $v'=\langle v^2\rangle^{1/2}$) values of axial and radial velocity fluctuation are shown in Fig. 3a and 3b. The maximum of turbulent intensity $u'/\langle u_c\rangle$ of the hydrogen jet is noticeably higher than for helium and has a clearly defined peak, reaching a maximum of approximately 0.61 at *x/D* = 5 and approach the asymptotic value of ~ 0.35 at *x/D* ~ 15, which confirms rapid convergence of the hydrogen jet to a self-similar mode. Transversal $v'/u_c$ component remains highly variable farther downstream than $u'/u_c$, approaching value of ~ 0.3 at *x/D* ~ 25. The resulting asymptotic ratio $v'/u' \sim$ 0.86, lie within the range of values cited in the literature for jets ejected from contraction nozzle [16]. Figure 4a shows the inverse hydrogen mass fraction at the centerline as a function of a distance from the jet origin. Jet concentration along the centerline obeys the relation [17]

$$Y_j / < Y_c >= K_c \frac{x - x_{voy}}{r_e}, \tag{8}$$

where $r_e = r\left(\rho_j / \rho_\infty\right)^{1/2}$ is the effective radius of the jet and $x_{voy}$ is the virtual origin calculated from mass fraction centerline evolution. An extension of this relation for the flows with global density variations can be written as $Y_j / < Y_c >= K_c x / r_e + \left[\left(\rho_\infty / \rho_j\right) - 1\right] K$ [5], with constant $K$ being negative. Analysis of the data shown in Fig. 4 provides values $K_c$=0.262 and $K$=-0.151. The jet growth as determined by half-width $L_y$ is linear, with growth rate somewhat higher for the scalar field compared with velocity field.

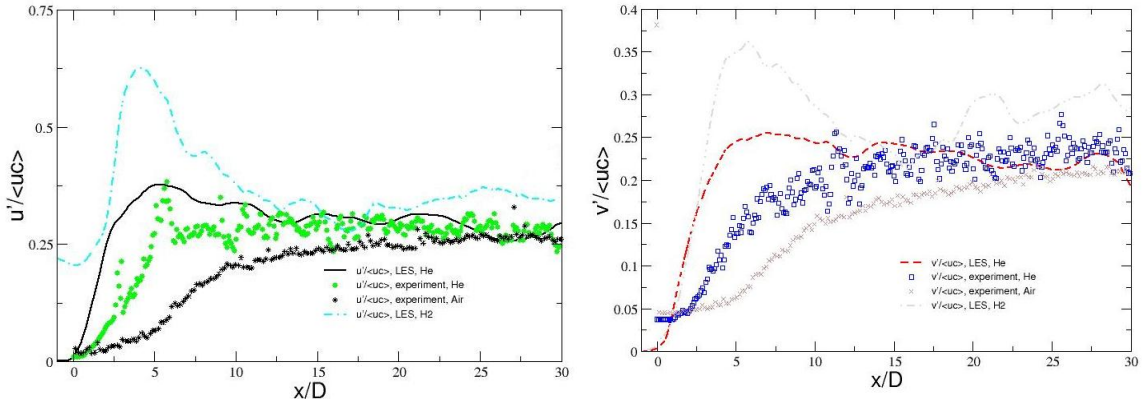


Figure 3. a) RMS to mean axial velocity ratio *u'/<u$_c$>* *versus x/D* at jet centerline. PIV and LES; b) Transversal RMS to mean velocity ratio *v'/<u_c>* *versus x/D* at jet centerline. PIV and LES

Figure 4b illustrates the ratio of the helium mass fraction RMS to the centerline mean mass fraction value Y'/<$Y_c$>, sometimes referred to as an unmixedness value. The peak unmixedness value is again noticeably higher than the one for helium (~ 0.75 *versus* ~ 0.45) and takes longer to decline toward the asymptotic value of ~ 0.29 - 0.30, similar to the one observed for the helium jet. It appears to recommence the slight decrease at the end of the computational domain for both gases. The higher peak unmixedness value of hydrogen potentially indicates the possible higher influence of buoyancy, e.g. through the enhanced entrainment.

Figure 5a shows self-similar collapse of the helium mass fraction profiles normalized by jet half-width $L_y$. Non-buoyant jets mixing can be approximated by the Gaussian curve. The deviation of mass fraction profiles in Fig.6a, visible toward the edges of the jet (hydrogen/air interface zone) can be explained by the effects of buoyancy on the velocity field in the shear layer, affecting mixing process [4], [18]. The extent of deviation is comparable to the one observed for the helium jet [10].

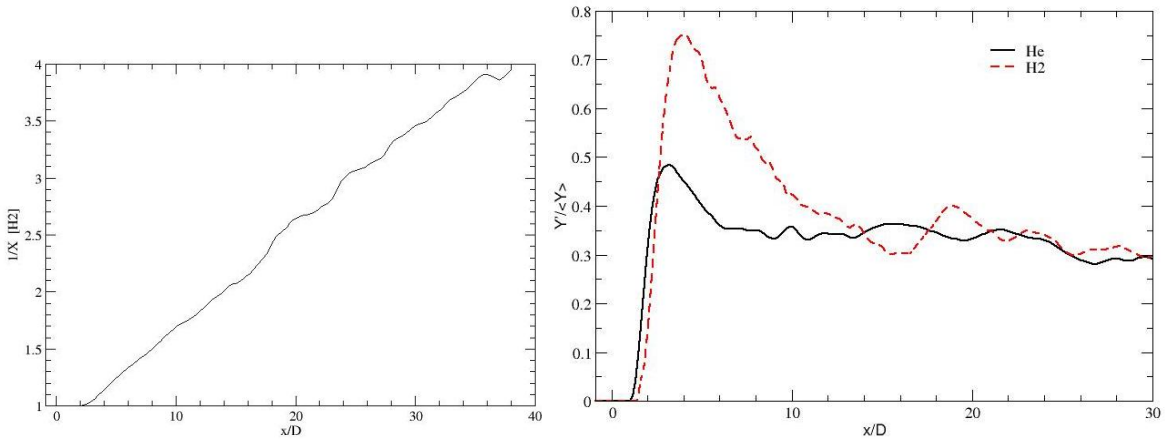


Figure 4. a) Jet spread molar fraction $X_j/X_c$ *versus x/D*; b) RMS to mean mass fraction ratio (unmixedness) $Y'/\langle Y_c \rangle$ *versus x/D* for hydrogen and helium.

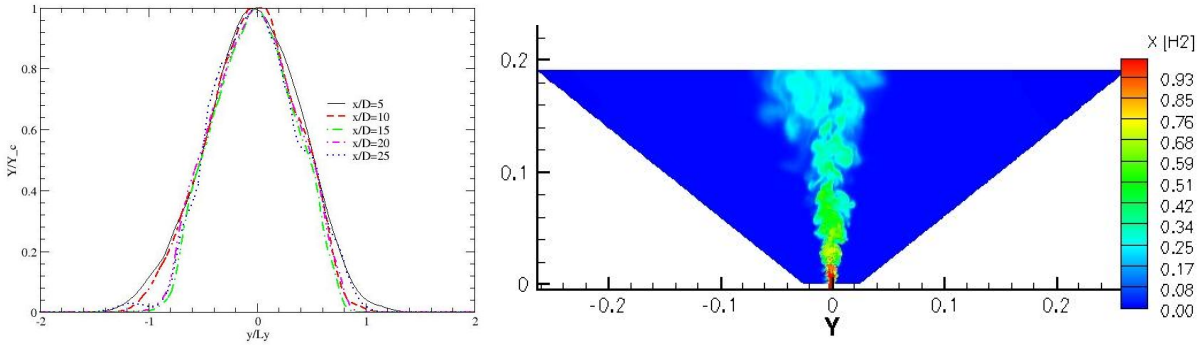


Figure 5. a) Normalized mean concentration (hydrogen mass fraction) profiles $\langle Y \rangle/\langle Y_c \rangle$ *versus* $y/L_y$ at various distances from the nozzle *x/D;* b) Instantaneous hydrogen molar fraction filed.

### 3.2 Transient Concentration Fields: Frequency of Flammable Condition Occurrence

One of the primary results of helium jet release study [10] was an observation of transient pockets of gas with concentration within flammability limits. The monitoring of these transient concentration fields is important for evaluation of safety margins for the emergency hydrogen release case, since even the transient increase of hydrogen concentration above flammability threshold near ignition source can be sufficient to initiate combustion, despite the time-averaged concentration value at the this location being below the threshold. It has been shown that account for such transient gas pockets can significantly increase the extent of potentially flammable gas envelope. Present work extends these results from helium standing for combustible gas to the hydrogen, and further investigates the structure and characteristics of this extended envelope. These transient eddies of high concentration of flammable gas are driven by a combination of the turbulence and the hydrodynamic instabilities, including transversal jet oscillations and vortex generation and shedding at the mixing layer. Indeed, an instantaneous snapshot of the concentration field reveals complex pattern (see Fig. 5b), with a number of pockets of flammable gas with concentration exceeding flammability threshold observed outside the average flammability threshold. It is therefore necessary, in order to establish proper safety margins to take into account transient concentration fields as well as the average filed. Note that the term 'flammable condition' in the present work refer only to the gas concentrations within flammability limits, and do not take into account flow velocity, turbulence level, temperature, etc.,

which might inhibit ignition. LES approach, with its accurate modeling of the turbulent effects, is particularly well suited for investigation of such transient phenomena.

In order to assess the extent and persistence of the transient concentration field numerical simulations recorded cumulative data on the distribution of the areas of gas concentration within flammability limits (taken as lying within 4 – 75% by volume [19], for the case of helium jet [10], calculation of the transient envelope assumed same "flammability" limits as for hydrogen). Data collection has been performed at regular intervals for four flowthrough time periods. The ratio of samples in which concentration in a given cell lied within flammability threshold, to the total number of samples, is referred to as a frequency of flammable condition occurrence in a given cell, and characterize persistence of the flammable conditions. Present work concentrated on the momentum dominated near field of the jet ($X/D$ < 30 for the present work), encompassing transition from the potential flow and the initial stages of the self-similar expansion. Note that while transient effects are expected to play a lesser role in the momentum dominated area when compared to the far field where buoyancy and turbulence effects become dominant, it is nevertheless an important region due to its proximity to the storage tank and potential ignition sources.

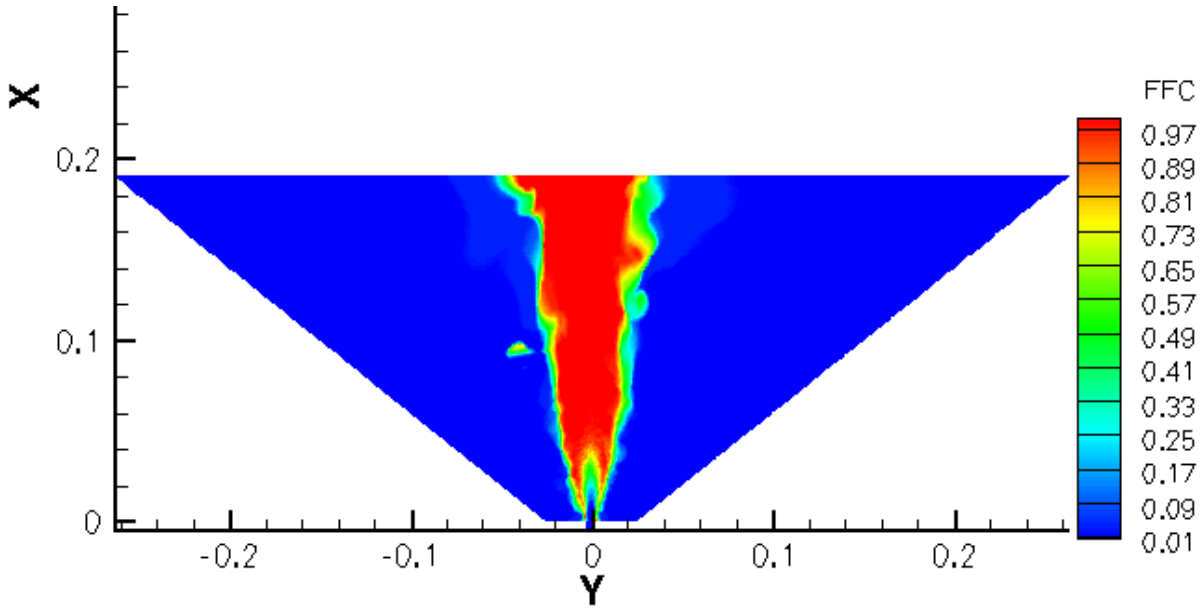


Figure 6. Spatial distribution of the cells with hydrogen concentration within flammability limits. Colours denote the frequency of occurrence of flammable conditions (FFC).

Figure 6 illustrates the frequency of hydrogen flammable condition (FFC) occurrence in jet cross-section. Red area in the core of the jet corresponds to the area of persistent hydrogen concentration (FFC = 1) within flammability limits. It can be seen that the account for transient flammable zones (FFC > 0) can increase the extent of the flammability zone by up to 50%. The area of the hydrogen concentration exceeding upper flammability threshold is relatively small, but nevertheless significant as it is occurs in the immediate vicinity of the storage tank and potential ignition sources. It can be seen that the persistent region of excessive (i.e., above upper flammability threshold) concentration is confined to the cylinder with diameter not exceeding initial nozzle diameter and terminating near the point of the beginning of jet transition from the potential flow to the self-similar mode, at approximately 2 $x/D$. The transient region of excessive gas concentrations extends significantly further, up to ~8 $x/D$. Figure 7a illustrates frequency of the flammable condition occurrence at five distances from the nozzle, $x/D$ = 2, 5, 10, 15 and 20, normalized by $L_y$. It illustrates the significant

extent of area with excessive transient concentration values at *x/D* = 5, while Fig. 7b shows the frequency of excessive hydrogen concentration occurrence at the jet centerline.

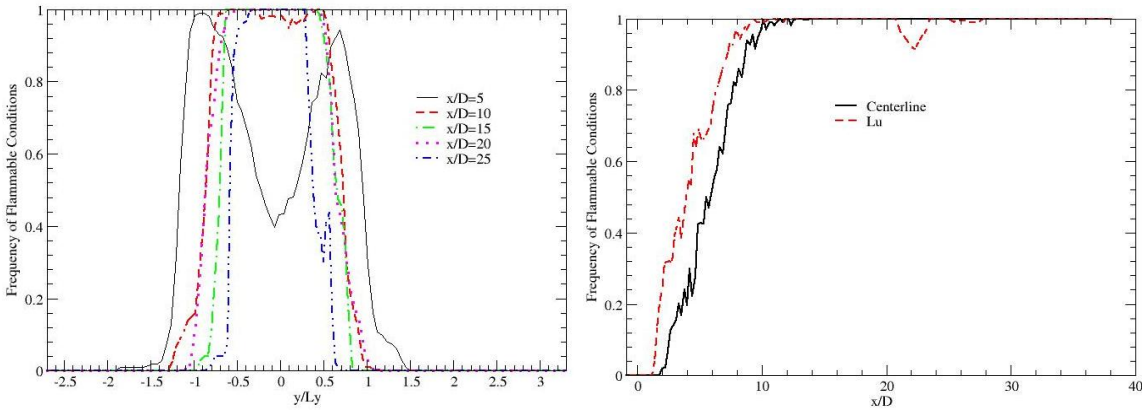


Figure 7. a) Frequency of flammable conditions occurrence at various distances from the nozzle *x/D* normalized by $L_y$; b) Frequency of the flammable condition occurrence along the jet centerline near the nozzle.

The implication of the transient concentration fields for the safety guidelines is summarized in Fig. 8. Figure 8a shows the evolution of the maximum extent of the flammable conditions observed during numerical simulation ($L_{fmax}$), and the jet width as defined by the extent of the persistent flammable condition (i.e., all samples show concentration within flammable range) ($L_{pf}$). Figure 8b shows $L_{fmax}$ and $L_{pf}$ normalized by $L_y$ jet width, and compared with the results for helium jet. It is seen that the results are close (outlier point at *x/D*=20 for helium is likely caused by influence of the boundary which was closer for helium case). It can be seen that the $L_{fmax}/L_y$ monotonously decreases, indicating that, as centerline concentration values drop, the flammability limit approaches $L_y$ jet boundary. $L_{pf}$ curves exhibit similar behavior toward the outlet boundary, but are suppressed near the nozzle where the hydrogen concentration at the centerline exceeds upper flammable threshold. $L_{pf}$. closely matches jet width $L_u$ derived from velocity, being confined to the core of the jet, inside of the mixing layers. The evolution of the transient flammable concentration envelope expanse can be responsible for the observation reported in [12], that at M ~ 0.2 the minimal hydrogen concentration for ignition was 6.4-7.5% rather than 4%, which was attributed to influence of the transient eddies with lean hydrogen mixture. The ratio between $L_f$, and $L_{pf}$. varies in a range of 30% to 50%.

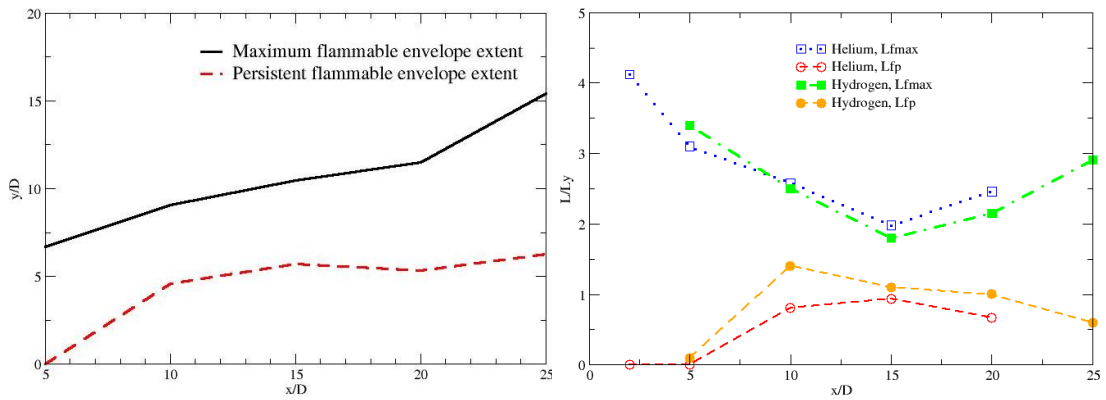

Figure 8. a) Maximum flammable gas concentration extent $L_{fmax}$ and the extent of persistent flammable gas concentration $L_{pf}$; b) Maximum flammable gas concentration extent $L_{fmax}$ and the extent of persistent flammable gas concentration $L_{pf}$ normalized by $L_y$ for hydrogen (solid markers) and helium (empty markers) jets at M=0.3.

### 3.3 Transient Concentration Fields: Characterization of Time-Resolved Concentration Fields

Having establishing the importance and averaged extent of transient flammable concentration fields, the next step is to attempt to characterize the transient gas pockets composing this extended envelope. Figure 9 shows instantaneous snapshots of concentrations fields illustrating the complex nature of these pockets. As can be seen, highly turbulent jet is composed from a number of individual eddies. Observation of concentration profiles behaviour in X-Y cross-sections at *x/D*=2, 5 and 10 helps to characterize the frequency of appearance and extent of the transient gas pockets carried by these eddies (Fig. 10).

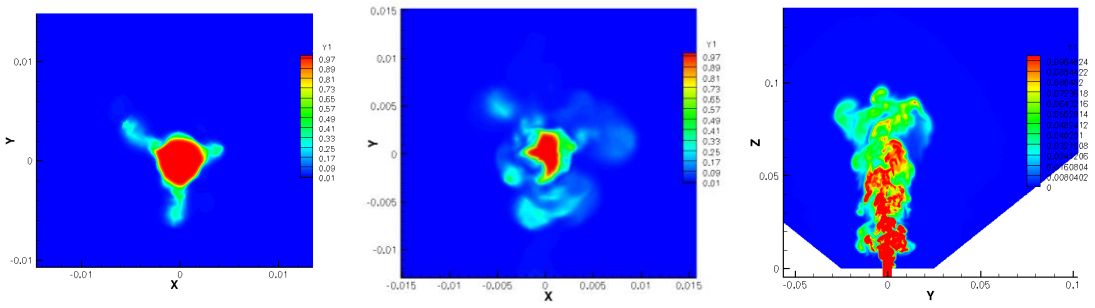

Figure 9. Instantaneous hydrogen concentration fields at a) *x/D=2*; b) *x/D=5*; c) along the jet centerline;

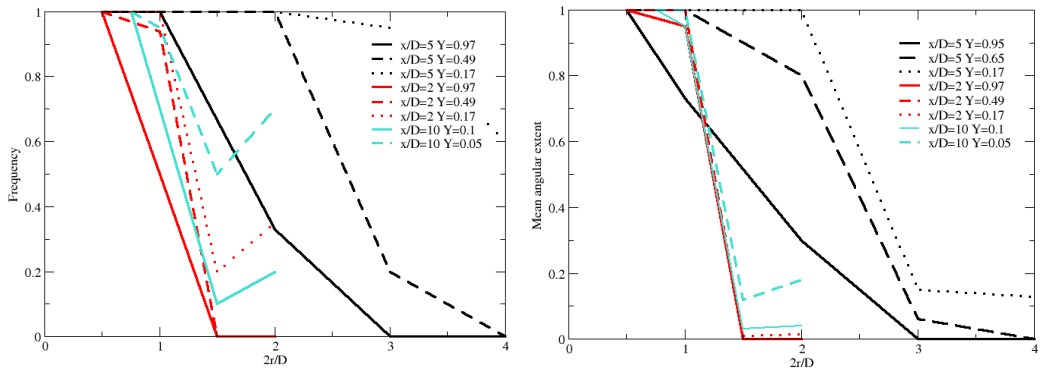


Figure 10. a) Frequency of gas pockets with hydrogen mass fraction exceeding specified *Y* values; and b) mean angular extent of pockets of gas with hydrogen mass fraction exceeding specified *Y* value, at *x/D*=2, 5 and 10 *versus* radial extent from the centerline.

Observation of time evolution of the jet in cross sections at both *x/D*=2 and *x/D*=5 contain regions where hydrogen concentration exceed upper flammability threshold near the jet centerline, while at *x/D*=10 conditions are always flammable within the jet core. The character of transient behaviour also changes as one moves further from the jet origin. At *x/D*=2 almost the entire jet core has its

concentration above the flammability threshold. The flammable concentrations appear in relatively small peripheral branches, narrowly connected to (and periodically completely separating from) jet core. The core of the jet, still consisting of almost entirely pure hydrogen retains a close to circular shape, and is surrounded by a pulsating zone (with hydrogen concentration 92...97%), which at maximum extent doubles the radius of the core. The boundary is fairly sharp and the combustible envelope is very thin. This roughly circular pulsing core is periodically surrounded by flammable pockets, appearing as narrow but long extrusions, which often get separated entirely, leaving detached gas pockets. These pockets persist for extended duration. This behaviour is illustrated in Figure 10, which introduces two integral parameters, facilitating characterisation of persistence and angular extent of such outliers. The frequency parameter (Fig. 10a) characterize the percentage of time during which a given concentration value has been observed at a given radius from the jet centerline (at any portion of its circumference). It is seen, that for $x/D$=2 case the high concentration core is mostly persistent, as are outlying pockets of flammable concentrations, while intermediate protrusions have relatively low lifetime. The mean angular extent parameter (Fig. 10b) indicates what average percentage of total circumference of a given radius contained mass fraction of hydrogen above a given value $Y$ (the averaging is performed only for the time when a given gas concentration was present, to avoid introducing frequency influence). From the plots for the $x/D$=2 cross section, it is seen that the entire core is roughly circular, while both flammable pockets and extrusions are very thin, occupying only small part of the circumference. This indicates that while the extent of the flammable zone is significantly extended by these extrusions, they occupy relatively small angular space, and the shape of flammable zone is highly asymmetric. At $x/D$=5 the central hydrogen core is fully destabilized, and changes its shape and extent with high frequency. It is surrounded by zone of high (~90%) hydrogen concentration, which is also highly dynamic, and exhibit strong asymmetric excursions. Combustible region reach much greater extent, being primarily composed of semi-separated clouds which exhibit relatively low mobility compared to highly dynamic core. Their angular coverage has greatly expanded , although they still do not completely surround the jet core. Finally at $x/D$=10 the pure hydrogen core with hydrogen concentration exceeding upper flammability threshold disappears, leaving the core of flammable gas concentration. Rather than exhibiting pulsation covering most of circumference, its dynamics consists mostly of producing and releasing extrusions (which are much thicker than similar features at $x/D$=2), which after separation leave flammable gas concentration pockets persisting for an extended durations. The flammable region, therefore, consists of a combination of persistent central core, highly transient and relatively narrow extrusions, and long lived but relatively narrow separated gas pockets, which at maximum extent can triple the width of flammable envelope. These observations indicate that transient envelope, rather than being a pulsating sheath surrounding the persistently flammable jet as can be inferred from Fig. 6 and 7, with low frequency corresponding to low duration of presence of flammable concentrations in the area, can in fact consists of individual pockets with relatively long lifetime but occupying relatively small fraction of circumference at a time. The practical implication is that the areas showing low frequency of flammable condition in Fig. 6 are still need to be considered for safety purposes, since they can persist for a sufficiently long time to support the ignition.

### 3.4 Effect of the LES Grid Resolution on Transient Concentration Field Simulation

The previous sections illustrated the usefulness of high-fidelity numerical tool for analyzing of true extent of potentially flammable hydrogen concentration envelop extent. Unfortunately, even in the age of high-performance parallel computation facilities, the properly resolved LES requires resources which often exceed the practical limits for industrial applications, which are often called to perform a large number of simulation of variety of cases in limited timeframe. Another related problem is the necessary reduction of the computational domain extent - e.g., the present research has been restricted to momentum dominated near field, while many practically important phenomena take place at a significantly greater extent at hundreds nozzle diameters from point of origin. One of the potential ways to circumvent these limitations is to reduce grid resolution, increasing the threshold of

unresolved subgrid scales. One of the main problems of this approach is the ambiguity of validation grid resolution selection. While it is possible to directly compare averaged data obtained on different grids, turbulent properties calculated of LES are dependent on the filter size which represent significant difficulty in selecting a metric for comparison of transient results obtained for different grids. In order to avoid this problem in the present study, a grid resolution influence on the extent of the transient flammable gas envelope, described in previous sections, has been chosen to serve as an indicator of grid suitability for obtaining practically relevant results. This allows one to perform a direct comparison of results of the practical interest dependent on a proper turbulence modelling. A built in feature of SPARC, which allowed gracefully double grid resolution from within simulation has been used to ensure the correct comparison. The results are shown in Fig. 11. The averaged axial quantities proved to be the most robust, showing a reasonable agreement between all cases. It becomes immediately apparent, however, that the two lowest order grid did not provide good turbulence modelling (as indicated by a relatively smooth appearance of corresponding curves - compare with the difference between averaged and instantaneous data for 3rd level grid). This observation was further supported by comparison of the extent of the flammable envelope (similar to presented in Fig.8b) between different grid levels (see Fig. 11b). Two lower resolution grids dramatically underestimated the extent of flammable envelope, with the results being close to ones being based on averaged concentration values - i.e., ignoring transient outliers completely. This observation emphasizes the critical importance of providing adequate grid resolution at least in the vicinity of transition and early self-similar region in order to realistic simulation of transient gas pockets, posing potential ignition hazard.

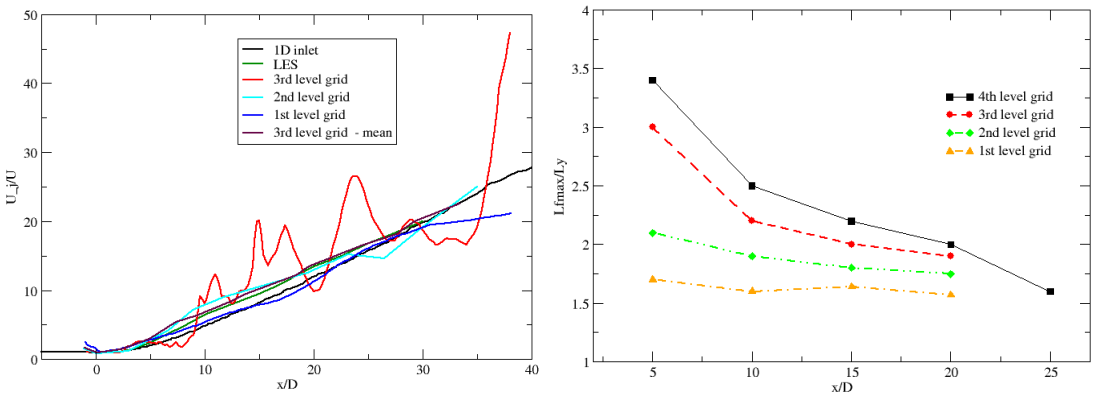


Figure 11. a) Comparison of axial velocity decay computed on different grids (each decrease in grid level represent doubling of cell sizes in each direction). Both instantaneous and averaged values are shown for 3rd level grid; b) Comparison of the normalized maximum extent of flammable concentration field for four grid levels..

## 4.0 CONCLUSIONS

Numerical and experimental investigation of the hydrogen jet has been performed with the aim to investigate the extent and structure of transient concentration fields. The axial velocity and scalar mass fraction evolution showed behavior consistent with obtained in the previous simulations and reported in the literature. Turbulence intensity and mass fraction variance along the centerline demonstrated higher mixing intensity than was previously obtained for helium jets. Investigation of the transient concentration fields exceeding hydrogen flammability limit indicated that transient flammable region adds approximately 25-30% to the radius of averaged flammable volume. It has a complex spatial structure, resulting in the potentially sufficiently long for ignition presence time for gas pockets with flammable concentrations within the entire area of potentially flammable envelope. The persistent flammable concentration volume has been shown to roughly coincide with the jet core, with the radius

of 30-40% of the maximum extent of transient flammable filed. Alternative less computation intensive approaches were explored and demonstrated acceptable prediction of extent and behavior of averaged parameters along jet centerline, but was found lacking in transient fields prediction.

## 5.0 ACKNOWLEDGEMENTS

This work was supported by the NSERC H2Can Research Network and Natural Resources Canada.

## REFERENCES

1. K. Harstad and J. Bellan., Global analysis and parametric dependencies for potential unintended hydrogen-fuel releases, *Combustion and Flame*, **144**, 2006, pp. 89-102.
2. M. Amielh, T. Djeridane, F. Anselmet and L. Fulachier, Velocity near-field of variable density turbulent jets. *Int. J. Heat Mass Transfer*, **39**, No.10, 1996, pp. 2149--2164.
3. R. M. C. So, J. Y. Zhu, M. V. Otugen, and B. C. Hwang, Some measurements in a binary gas jet , *Experiments in Fluids*, **9,** 1990, pp. 273-284.
4. D. B. Helmer and L. K. Su. Imaging of turbulent buoyant jet mixing. AIAA Paper 2006-309, 44th Aerospace Sciences Meeting and Exhibit, 9-12 January 2006, Reno, NV.
5. W. M. Pitts, Effects of global density and Reynolds number variation on mixing in turbulent axisymmetric jets, Nat. Bur. Stand., NBSIR 86-3340.
6. J. R. DeBonis and J. N. Scott., Large eddy simulation of a turbulent compressible round jet, *AIAA Journal*, **40**, No.7, 2002, pp. 1346-1354.
7. H. Suto, K. Matusara, M. Kobayashi, and Y. Kaneko, Large Eddy Simulation of flow and scalar transport in a round jet, *Heat Transfer - Asian Research*, **33**, No.3, 2004, pp. 175-188.
8. K. Mohamed and M. Paraschivoiu, Real gas simulation of hydrogen release from a high-pressure chamber, *Int. J. Hydrogen Energy*, **30**, No.8, 2005, pp. 903-912.
9. W. M. Pitts, Effects of global density ratio on the centerline mixing behavior of axisymmetric turbulent jets, *Experiments in Fluids*, **11**, 1991, pp. 125-134.
10. B. Chernyavsky, T.C. Wu,F. Peneau, P. Benard, P. Oshkai and N. Djilali, Numerical and experimental investigation of buoyant gas release: Application to hydrogen jets, *Intl. J. of Hydrogen Energy*. **36**, No.3, 2010, p. 2645-2655.
11. W. Houf, R. Schefer, Predicting radiative heat fluxes and flammability envelopes from unintended releases of hydrogen, *Intl. J. of Hydrogen Energy*. **32**, No.1, 2007, p. 136-151.
12. M. R. Swain, P. A. Filoso, M. N. Swain, An Experimental investigation of ignition of leaking hydrogen, *Intl. J. of Hydrogen Energy*. **32**, No.2, 2007, p. 287-295.
13. F. Magagnato, KAPPA – Karlsruhe program for aerodynamics, TASK quarterly, 2 (2), 1998, pp. 215-270.
14. W. C. Reynolds, Fundamentals of turbulence for turbulence modeling and simulation, *Lecture Notes for Von Karman Institute* Agard Report No. 755, 1987.
15. R. K. Chen and W. Rodi, Vertical Turbulent Jets,1980, Pergamon Press, Oxford.
16. G. Xu and R. A. Antonia, Effect of different initial conditions on a turbulent round free jet, *Experiments in Fluids*, **33**, 2002, pp. 677-683.
17. M. W. Thring and M. P. Newby, Combustion length of enclosed turbulent jet flames, Fourth Symposium (International) on Combustion, Pittsburgh: The Standing Committee on Combustion, 1953, pp. 786-796.
18. C. Niwa, J. Ichizawa, N. Yoshikawa, and K. Ohtake, Time-resolved concentration measurements of jets by laser Rayleigh method - comparison of He, $CO_2$ and $CCl_2F_2$ jets. Proceedings of the Fourteens International Symposium on Space Technology and Science, Tokyo, 1984, pp. 469-476.
19. M. G. Zebatanis, US Bureau of Mines, Bulletin 627, 1965.